# Preliminary Analysis of a Biologically Inspired 1-DOF "Clock" Stabilized Hopper*

**Haldun Komsuoğlu** (hkomsuog@umich.edu)
**Daniel E. Koditschek** (kod@umich.edu)
**Department of Electrical Engineering and Computer Science, The University of Michigan**
**Ann Arbor, MI 48109-2110, USA**

## ABSTRACT

We investigate the stability of a one degree of freedom mechanical spring-mass system modulated by a feedforward "clock" that stiffens and relaxes a Hooke's law potential force according to a periodic rhythm. At the present early stage of inquiry, we offer sufficient conditions for local asymptotic stability of an isolated periodic orbit when there is no feedback to the clock at all but some viscous friction in the mechanism. We conjecture that, absent feedback, a lossless mechanical system cannot exhibit an asymptotically stable limit cycle in response to such rhythmic excitation.

**Keywords:** legged locomotion, coupled oscillators, clock driven system, CPG, feedforward control, biomechanics, spring-mass model

## 1. INTRODUCTION

The motivation for this inquiry arises from a practical problem in robotics, inspired, in turn, by our reading of the biological literature. A recently reported set of experiments [3, 19] demonstrate that a simple compliant leg hexapod robot, completely open loop with respect to any task level perception, can negotiate widely varied and dramatically adversarial terrain when its leg motors are driven by a purely feedforward "clock" reference signal. At present, no analytical machinery is available that can inform directly our efforts to improve and refine this device, specifically with regard to the introduction of simple task level sensors for the purpose of instrumenting low bandwidth feedback. The results reported here represent our first steps toward that end.

Originating with Wilson's [20] seminal analysis of insect leg coordination, scientists have identified a spectrum of biologically inspired coordination control strategies whose two extreme endpoints we wish to examine analytically. On the one hand a "reflex" based perspective [4,5] stresses the key role of sensory data in mediating the control signals sent to an animal's muscles. Alternatively, the "clock" [8,11,12,14] view of animal motion control stresses the role of pattern generation — periodic reference trajectories that act as feedforward control signals — in the coordination of such cyclic behaviors as walking, running, and so on. The robotics literature also explores a comparable spectrum of coordination approaches from reflex [2, 15] through pure clock [16, 17]. In a recent paper [10] the second author and colleagues re-examine the "reflex" end of this coordination spectrum in the specific context of locomotion. In this paper, we are concerned more with the "clock" end. To the best of our knowledge Berkemeier and colleagues [1] comprise the only previous group that has explored analytically the issue of a clock stabilized 1 dof mechanism. That work addresses a similar coupled system, utilizing rest length as the control input, and introducing approximate return maps derived by perturbation methods. Unfortunately, such perturbation techniques are guaranteed to work only for very small values of the damping coefficient — what appears to be the ultimate source of stability in the first place. In this paper we provide closed form exact return maps from which we derive sufficient conditions for local stability that are easily related to the physical parameters yielding guaranteed behavioral conclusions over the broad range of the model's operation.

A second motivating influence from the biological literature concerns the model of actuation. Hill's classical view [7] of muscle presents a combination of a nonlinear passive spring and an "active" component that generates additional force based on the motor commands [13]. A phenomenological view, characteristic of the biomechanics community, has lead to studies of in vivo locomotion behavior suggesting that effective leg stiffness is altered by the motor nervous system to adapt to external disturbances and control gait [6]. Altering the gait through changes in the available potential energy has a long history of success in the robotics literature as well [15]. For this reason, our simple model posits a stiffness control, again, in contrast to the model in [1].

*This work is supported by DARPA/ONR: N00014-98-1-0747.

## 2. THE SETTING

### A 1-DOF Hooke's Law Hopper with Adjustable Stiffness

We consider a one degree of freedom (mechanical) hopper[1] on a real interval, $\mathcal{X}_1 \subseteq \mathbb{R}$, that consists of a point body mass and a massless (Hooke's Law) springy leg pointing downward. Letting $\mathcal{X} := T\mathcal{X}_1 = \mathcal{X}_1 \times \mathbb{R}$, define the contact set, $\mathcal{G} := \{x \in \mathcal{X} | x_1 < 0\}$, with stance (or contact) mode[2]

$$\dot{x} = f_p(x) = \begin{bmatrix} x_2 \\ -px_1 - bx_2 \end{bmatrix}, \quad x \in \mathcal{G} \tag{1}$$

and *aerial mode*,

$$\dot{x} = f_{\mathcal{L}}(x) = \begin{bmatrix} x_2 \\ -1 \end{bmatrix}, \quad x \in \mathcal{L} := \mathcal{X} - \mathcal{G}, \tag{2}$$

where the control takes the form of an "adjustable" stiffness, $p \in \mathcal{P} := \mathbb{R}^+$.

### A Clock-Based Switching Controller

We posit a controller in the form of a one dimensional tunable "clock" — a system defined on the circle, $\theta \in S^1$,

$$\dot{\theta} = w_c = \frac{2\pi}{T_c}, \tag{3}$$

whose state, $\theta$, is filtered by an output function, $\kappa(\theta)$. In order to obtain a periodic pulse train, $o(t)$, we define $\kappa(\theta) := p_o + \Delta p[unit(\theta) - unit(\theta - w_c\beta)]$, where "$unit(\theta)$" denotes the unit step function. Four parameters define the control signal: controller period, $T_c$; forcing duration, $\beta$; offset value, $p_o$; and forcing increment, $\Delta p$, as depicted in Figure 1. Denote by $\mathcal{B} := \{(\Delta p, \beta) | \Delta p > 0 \wedge \beta \in (0, \pi)\} = \mathbb{R}^+ \times (0, \pi)$ the physically meaningful forcing parameter space.

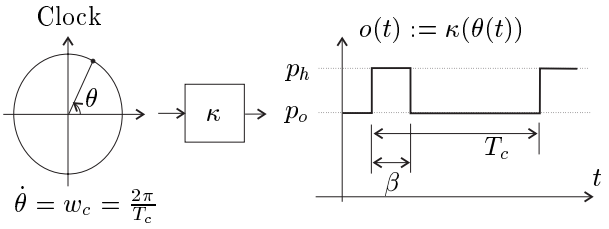


Figure 1: The clock-based switching controller.

### The Clock Controlled 1-DOF Hopper

The *clock controlled hopper* is obtained by simply connecting the output of the clock-based switching controller, $o(t)$, to the input of the mechanical hopper system, $p$, as depicted in Figure 2. There results an autonomous three dimensional hybrid dynamical system, $\dot{q} = F(q)$ where $q = [x_1, x_2, \theta]^T \in \mathcal{Q} := \mathcal{X} \times S^1$. In this coupled system the control actions are limited to the (physically unrealistic but illustrative) binary choice of $p \in \{p_o, p_h\}$ representing a "relaxed," $p_o \in \mathcal{P}$, and a "stiffened," $p_h := p_o + \Delta p \in \mathcal{P}$ force profile. Although the resulting discontinuities in the vector field preclude the standard guarantees of existence and uniqueness [9], we will avoid distracting technical considerations by bounding from below the magnitude of the time intervening between successive control actions, i.e. $T_c > \beta > 0$.

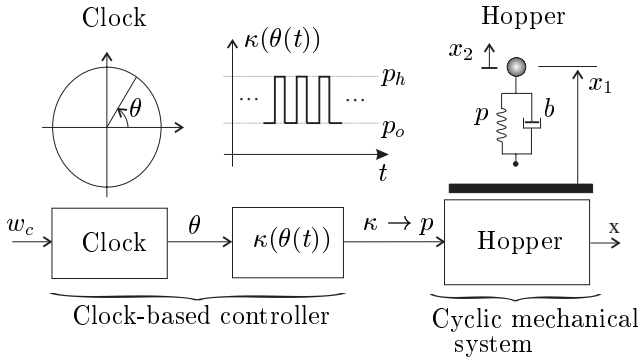


Figure 2: Clock controlled 1-DOF hopper.

## 3. DERIVATION OF THE RETURN MAP

### Continuous-Time Dynamics and Associated Transformations

The clock controlled hopper is a hybrid dynamical system, whose coupled state space, $\mathcal{Q}$, will be partitioned into three "modes":

$$\begin{aligned}
&\text{a normal (stance) mode, } \mathcal{N}, \\
&\dot{q} = \begin{bmatrix} f_{p_o}(x) \\ w_c \end{bmatrix}, q \in \underbrace{\{q \in \mathcal{Q} | \theta \in (w_c\beta, 2\pi) \wedge x \in \mathcal{G}\}}_{\mathcal{N} :=}; \\
&\text{a forced (stance) mode, } \mathcal{F}, \\
&\dot{q} = \begin{bmatrix} f_{p_h}(x) \\ w_c \end{bmatrix}, q \in \underbrace{\{q \in \mathcal{Q} | \theta \in [0, w_c\beta] \wedge x \in \mathcal{G}\}}_{\mathcal{F} :=}; \\
&\text{and a flight mode, } \mathcal{A}, \\
&\dot{q} = \begin{bmatrix} f_{\mathcal{L}}(x) \\ w_c \end{bmatrix}, q \in \underbrace{\{q \in \mathcal{Q} | x \in \mathcal{L}\}}_{\mathcal{A} :=}.
\end{aligned} \tag{4}$$

We prefer to study the mechanical component (hopper) stance behavior in a normalized coordinate system. The linear transformation,

$$g_p : \mathcal{X} \to \mathcal{Y}_p, \quad y = g_p(x) = G_p x, \quad G_p = \begin{bmatrix} \xi_p & \mu/\xi_p \\ 0 & \gamma_p/\xi_p \end{bmatrix}$$

itself parametrized by $p$ (where $\xi_p = \sqrt{p}$, $\mu = b/2$, $\gamma_p = \sqrt{\xi_p^2 - \mu^2}$), yields the Real Jordan Canonical form of the

[1] This system is presented in dimensionless coordinates, $x = [x_1, x_2]^T \in \mathcal{X}$, with dimensionless time, $t$.

[2] Gravitational acceleration is ignored during the stance mode.

linear vector field, Eq.(1), generating the familiar planar rotation and dilation expressions for the flow. This, in turn, motivates a passage to polar coordinates, leading to what we will term the *normalized energy-phase* coordinate system, $\mathcal{E} := \overline{\mathbb{R}^+} \times S^1$,

$$m : \mathcal{Y} \to \mathcal{E}, \quad e = \begin{bmatrix} \eta \\ \phi \end{bmatrix} = m(y) = \begin{bmatrix} ||y||_2 \\ \arctan(\frac{-y_1}{-y_2}) \end{bmatrix},$$

yielding dynamics,

$$\dot{e} = \tilde{f}_p(e) = \begin{bmatrix} -\mu\eta \\ \gamma_p \end{bmatrix}, \quad \tilde{f}_p^t(e(0)) = \begin{bmatrix} exp\,[-\mu t]\,\eta(0) \\ \gamma_p t + \phi(0) \end{bmatrix}, \tag{5}$$

that are conjugate to Eq.(1) via $\tilde{f}_p^t \equiv m \circ g_p \circ f_p^t \circ g_p^{-1} \circ m^{-1}$. One can always choose the dimensionless coordinate system, $\mathcal{X}$, so that $\gamma_{p_o} = 1$ and $\gamma_{p_h} > 1$, which we now assume.

These transformations affect neither the time nor the clock state, $\theta$, hence, for constant parameter, $p$, the coupled system dynamics in the new coordinate system, $c = [e,\, \theta]^T \in \mathcal{C}_p := \mathcal{E}_p \times S^1$, is obtained by appropriately augmenting Eq.(5) and Eq.(3).

$$\begin{array}{ccccc} & g_{p_o} \nearrow & \mathcal{Y}_{p_o} & \xrightarrow{m} & \mathcal{E}_{p_o} \\ \mathcal{X} & & & & \downarrow h \\ & g_{p_h} \searrow & \mathcal{Y}_{p_h} & \xrightarrow[m]{} & \mathcal{E}_{p_h} \end{array}$$

Figure 3: The induced change of coordinates, $h$, makes the diagram relating the normal and forced modes commutative.

The parametric dependence of $g_p$ on the normalized spring stiffness, $p$, causes the normalized coordinate systems for the normal mode, $\mathcal{Y}_{p_o}$, and the forced mode, $\mathcal{Y}_{p_h}$, to be different. As a consequence, their respective normalized energy-phase coordinate systems differ as well. The change of coordinates $h : \mathcal{E}_{p_o} \to \mathcal{E}_{p_h}$ is given by $e_{p_h} = h(e_{p_o}) = m \circ g_{p_h} \circ g_{p_o}^{-1} \circ m^{-1}(e_{p_o})$, as depicted in the commutative diagram of Figure 3, where we define,

$$h_1(e_{p_o}) := \eta_{p_o} \overbrace{\frac{\gamma_{p_h}\xi_{p_o}}{\gamma_{p_o}\xi_{p_h}} \cos(\phi_{p_o}) \sqrt{1 + [T_1 \circ \tan(\phi_{p_o})]^2}}^{\overline{h}_1(\phi_{p_o})}$$

$$h_2(\phi_{p_o}) := \arctan \circ T_1 \circ \tan(\phi_{p_o}), \tag{6}$$

introducing for convenience in the sequel the first of 4 affine maps, $T_1(s) := \frac{\gamma_{p_o}\xi_{ph}^2}{\gamma_{p_h}\xi_{po}^2} s + \frac{\mu}{\gamma_{p_h}} \left[1 - \left(\frac{\xi_{ph}}{\xi_{po}}\right)^2\right]$. The inverse function, $h^{-1}$, has the same structure as $h$ except that the parameters $p_o$ and $p_h$ are interchanged in the above formulae,

$$e_{p_o} = h^{-1}(e_{p_h}) = \begin{bmatrix} \eta_{p_h} \overline{h_1^{-1}}(\phi_{p_h}) \\ h_2^{-1}(\phi_{p_h}) \end{bmatrix},$$

$$\overline{h_1^{-1}}(\phi_{p_h}) := \frac{\gamma_{p_o}\xi_{p_h}}{\gamma_{p_h}\xi_{p_o}} \cos(\phi_{p_h}) \sqrt{1 + [T_1^{-1} \circ \tan(\phi_{p_h})]^2}.$$

For use in the sequel, we state two facts as established by direct computation.

*Lemma 1:* $h_2'(\phi) := \frac{dh_2(\phi)}{d\phi} = \frac{\gamma_{p_h}}{\gamma_{p_o}} \left(1/\overline{h}_1(\phi)\right)^2$

*Corollary 1:* $(h_2^{-1})'(\phi) := \frac{dh_2^{-1}(\phi)}{d\phi} = \frac{\gamma_{p_o}}{\gamma_{p_h}} \left(1/\overline{h_1^{-1}}(\phi)\right)^2$

**Details of the Return Map Derivation**

For our study, we choose to define a Poincaré section corresponding to the forcing start instant, characterized by $\theta = 0$, $\Sigma := \{c \in \mathcal{C}_{p_o} | \theta = 0\}$. The flow of the coupled system Eq.(4) has the property that all the state trajectories originating in $\Sigma$ will return to it after some finite time. Sampling on the event of return to $\Sigma$ relates the three dimensional continuous-time system Eq.(4) to its corresponding two dimensional discrete-time Poincaré map Eq.(8). The independent states in $\Sigma$ are $\eta_{p_o}$ and $\phi_{p_o}$, but we find it advantageous to work in an alternative energy-phase coordinate system; $\mathcal{R} := \overline{\mathbb{R}^+} \times S^1$ defined by $z : \mathcal{E}_{p_o} \to \mathcal{R}$,

$$r = \begin{bmatrix} v \\ a \end{bmatrix} = z(e_{p_o}) := \begin{bmatrix} exp\,[\mu(\phi - \phi_{TD})]\,\eta_{p_o} \\ \phi_{p_o} - \phi_{TD} \end{bmatrix}, \tag{7}$$

where $\phi_{TD} := \arctan(\mu/\gamma_{p_o})$ represents the touchdown boundary phase in $\mathcal{E}_{p_o}$. Notice that $v$ is the dimensionless touchdown velocity, and $a$ is the dimensionless delay in the time that the next forcing interval starts relative to the last touchdown instant[3]. Figure 4 illustrates a typical state trajectory of the coupled system projected onto $\mathcal{Y}_{p_o}$ coordinates.

Each returned state, $r \in \mathcal{R}$, can be assigned a unique "mode sequence" — a string over the alphabet $\{\mathcal{N}, \mathcal{F}, \mathcal{A}\}$, Eq.(4) — according to the sequence of modes that its future continuous-time trajectory passes through on the way to the next return. This defines a partition of $\mathcal{R}$ according to common mode sequence. We will concentrate on a specific mode sequence, $\mathcal{FNAN}$, and evaluate the corresponding return map, $n(r)$. Denote hopper state (in $\mathcal{R}$) at the $k^{th}$ Poincaré sample by $r_k$. The next Poincaré sample is given by $r_{k+1} = n(r_k) = z \circ N_2 \circ A \circ N_1 \circ F \circ z^{-1}(r_k)$ where the factors are defined as $N_1 := \tilde{f}_{p_o}^{T_{ST}}$ ($1^{st}$ normal stance), $F := h^{-1} \circ \tilde{f}_{p_h}^{\beta} \circ h$ (forced stance), $A := m \circ g_{p_o} \circ f_{\mathcal{A}}^{T_{FL}} \circ g_{p_o}^{-1} \circ m^{-1}$ (flight), $N_2 := \tilde{f}_{p_o}^{a_{k+1}}$, ($2^{nd}$ normal stance) The forcing mode, $\mathcal{F}$, starts right after the Poincaré sampling and lasts for a constant interval, $\beta$. In

[3] These useful return map coordinates, $v$ and $a$, were proposed to us by Prof. Philip Holmes in a personal communication.

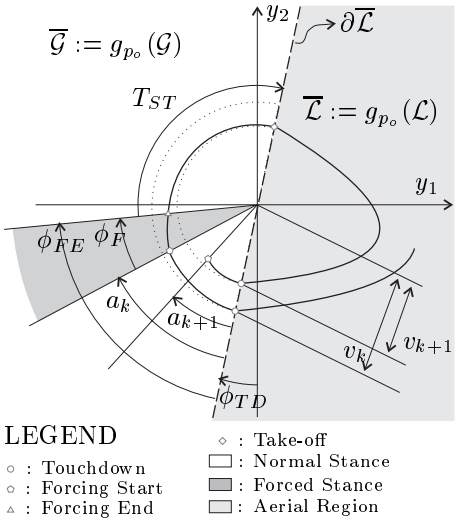


Figure 4: A typical hopping cycle viewed in the $\mathcal{Y}_{p_o}$ plane. Note that in $\mathcal{Y}_{p_o}$ the angle swept is equal to the time it takes to flow in the normal stance mode, $\mathcal{N}$.

this formula, $T_{ST}$ is the *remaining stance* time after forcing is concluded, and $T_{FL}$ is the time it takes to complete the following flight phase — both functions, in turn, of their respective initial conditions. Several properties of the intermediate maps will help us decompose this return map computation into two manageable steps, thereby affording computation of the component states, $v$ and $a$, independently.

*Proposition 1: The return map, restricted to mode sequence $\mathcal{FNAN}$, has the structure;*

$$r_{k+1} = n(r_k) = \begin{bmatrix} v_k\rho(a_k) \\ T_c - \beta - T_{ST}(a_k) - 2v_k\rho(a_k) \end{bmatrix}. \quad (8)$$

*where $T_{ST}(a)$ and $\rho(a)$ are defined in the proof below.*
*Proof:*
The mode sequence, $\mathcal{FNAN}$, models the physical situation where *each hopping cycle*[4] *has a unique forcing interval which starts and ends in the same stance mode.* Thus, the states whose forced trajectories experience these transitions along the way to the next return may be specified as

$$\mathcal{FNAN} := \mathcal{V} \cap (\pi_2 \circ n)^{-1}(\mathcal{V}) \quad (9)$$

where $\mathcal{V} := \{r \in \mathcal{R} | a \in [0, \alpha]\}$, and $\alpha$ is the unique root of $T_{ST}^{-1}(a) = 0$.

First, we derive the energy component of the return map[5], $n_1(r) := \pi_1 \circ n(r)$. Note that $\pi_1 \circ z \circ \tilde{f}_{p_o}^t(e) = id_{\overline{\mathbb{R}^+}}$, if $e \in \{e \in \mathcal{E}_{p_o} | \phi = \phi_{TD}\}$ (which corresponds to the touchdown boundary as depicted in Figure 4). Furthermore, since the flight is lossless and the take-off and touchdown heights are the same, we have $\pi_1 \circ m \circ g_{p_o} \circ f_{\mathcal{A}}^{T_{FL}} \circ g_{p_o}^{-1} \circ m^{-1} = id_{\mathbb{R}}$. Therefore, the only energy change occurs during the $k^{th}$ cycle stance, which consists of $\mathcal{NFN}$ modes from its touchdown to take-off, $n_1(r) = \pi_1 \circ \tilde{f}_{p_o}^{T_{ST}} \circ h^{-1} \circ \tilde{f}_{p_h}^{\beta} \circ h \circ z^{-1}(r)$. For ease of exposition in the sequel, we reorganize this expression exploiting the fact that $h_1$ (Eq.(6)) and $\pi_1 \circ z^{-1}$ (Eq.(7)) are linear in $\eta$ and $v$, respectively[6].

$$n_1(r) := v\rho(a), \quad \rho(a) := \varepsilon(a) l_1(a) l_2(a),$$

$$\begin{array}{lcl} \varepsilon(a) & := & exp\left[-\mu(a + \beta + T_{ST}(a))\right] \\ l_1(a) & := & \overline{h_1} \circ T_2(a) \\ l_2(a) & := & \overline{h_1^{-1}} \circ T_3 \circ h_2 \circ T_2(a) \end{array} \quad (10)$$

where $T_2(s) := s + \phi_{TD}$, and $T_3(s) := s + \gamma_{p_h}\beta$.

Second, we derive the phase delay component of the map, $n_2(r) := \pi_2 \circ n(r)$. Here, we exploit the fact that the time interval between two consecutive forcing start events is a constant, $T_c$. It follows that the intermediate time intervals must satisfy $\beta + T_{ST} + T_{FL} + a_{k+1} = T_c$, which yields $n_2(r) = T_c - \beta - T_{ST} - T_{FL}$. In normalized energy-phase coordinates, the angle swept by the state vector Eq.(5) is a linear function of time[7]. For the normal stance, $\gamma_{p_o} = 1$, $\Delta\phi = \Delta t$, therefore, the remaining stance time, $T_{ST}$, can be computed as $T_{ST}(r) := T_4 \circ \phi_{FE}(r)$, $T_4(s) := -s + \pi + \phi_{TD}$, using the forcing end phase, which is given by $\phi_{FE} := h_2^{-1} \circ T_3 \circ h_2 \circ T_2(a)$, yielding $T_{ST}(a) := T_4 \circ h_2^{-1} \circ T_3 \circ h_2 \circ T_2(a)$. The flight duration, $T_{FL}$, is a linear function of the take-off speed, which is also the touchdown speed for the next step, $T_{FL}(r_k) = 2v_{k+1} = 2v_k\rho(a_k)$.

## 4. RETURN MAP ANALYSIS

### Fixed Points

Fixed points of the return map, $n(r)$, must satisfy $n(r^*) = r^*$, which is equivalent to

$$\begin{array}{lcl} \rho(a^*) & = & 1 \\ v^* & = & \frac{T_c - \beta - a^* - T_{ST}(a^*)}{2} \end{array}, \quad r^* = \begin{bmatrix} v^* \\ a^* \end{bmatrix}. \quad (11)$$

Clearly, the existence and number of fixed points are governed by $\rho$, since the second formula in Eq.(11) simply evaluates the corresponding touchdown speed for a given forcing delay value, $a^*$. Recall, as well, that the return map, Eq.(8) is only valid for Poincaré states in the mode sequence $\mathcal{FNAN}$, so we must also require that $r^*$ is in that subset as well[8], as characterized in Eq.(9). We will call the fixed points of $n$ "valid" if and only if they are in this mode sequence. Figure 5 illustrates three different cases, where Eq.(8) can have one, two or no valid

[4] A hopping cycle is the interval between two consecutive touchdown events.

[5] Henceforth, we will refer to the projection onto the $i^{th}$ coordinate of any function, $f : \mathbb{R}^n \to \mathbb{R}^n$, either by $\pi_i \circ f$ or $f_i$.

[6] Note that $\varepsilon(a)$ models the total loss due to viscous friction in stance, while $l_1(a)$ and $l_2(a)$ represent the effects of the forcing start and forcing end parameter alternations, respectively.

[7] The delay and the angle are related by a linear function, $\Delta\phi = \gamma_p \Delta t$ in $\mathcal{E}_p$ (Eq.(5)).

[8] From Eq.(9) and Eq.(11) it follows that $a^* \in [0, \alpha] \Rightarrow r^* \in \mathcal{FNAN}$.

fixed points. Figure 6 summarizes the numerical parameter space study that illustrates the relationship between the existence of valid fixed points and the controller (forcing) parameters, $\Delta p$ and $\beta$.

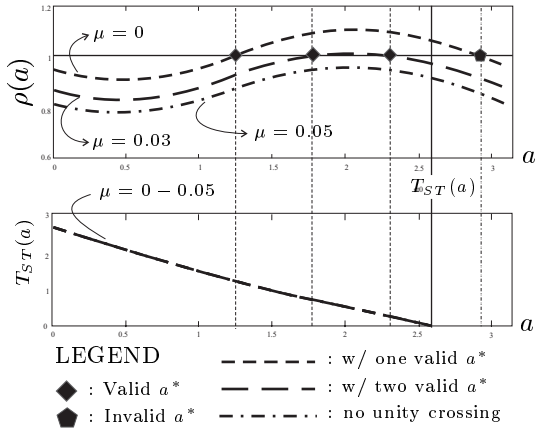


Figure 5: The plots of the $\rho(a)$ and $T_{ST}(a)$ functions ($\gamma_{p_h} = 1.2$ and $\beta = 0.5$) for three different $\mu$ values resulting in one, two and no valid fixed points.

*Conjecture 1: For any $\mu > 0$ there exists a non-empty set $\mathcal{B}_s(\mu) \subseteq \mathcal{B}$, such that for all $(\Delta p, \beta) \in \mathcal{B}_s(\mu)$, $\rho(a^*) = 1$ has real roots, and all the solutions, $a^*$, satisfy $|\rho'(a^*)| > 0$. Furthermore, there is a unique $a^* \in [0, \alpha]$ such that $\rho'(a^*) > 0$.*

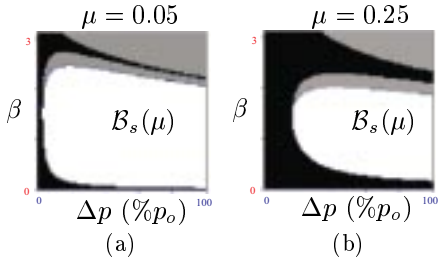


Figure 6: Numerical computation of $\mathcal{B}_s(\mu)$ for; (a) $\mu = 0.05$, (b) $\mu = 0.25$. The white region is the open set of parameter values, $\beta$ and $\Delta p$, yielding a unique valid fixed point satisfying $\rho'(a^*) > 0$. In the gray region, even though $\rho(a) = 1$ has roots, all of them are invalid. Finally, there is no $\rho(a)$ unity crossing for the parameter pairs in the black region.

**Local Stability Analysis**

The return map (Eq.(8)) must be linearized about the fixed points to determine local stability. The Jacobian of the return map evaluated at the fixed points is given by

$$J(r*) := Dn(r)|_{r^*} = \begin{bmatrix} 1 & v^*\rho'(a^*) \\ -2 & -T'_{ST}(a^*) - 2v^*\rho'(a^*) \end{bmatrix}$$

with two eigenvalues, $\lambda_\pm(v^*) = \frac{1}{2}\left(tr \pm \sqrt{\Delta}\right)$ where $tr := 1 - T'_{ST}(a^*) - 2v^*\rho'(a^*)$ is the the trace, and $\Delta := (1 - T'_{ST}(a^*) - 2v^*\rho'(a^*))^2 + 4T'_{ST}(a^*)$ is the discriminant of $J(r^*)$. The following results obtain from direct computation

*Lemma 2: The determinant of the Jacobian at the fixed points is $|J(v^*, a^*)| = -T'_{ST}(a^*)$.*

*Lemma 3: The first derivative of $T_{ST}(a)$ with respect to $a$ is related to $\rho(a)$ (Eq.(10)) by*

$$\frac{dT_{ST}(a)}{da} = -\left(\frac{1}{l_1(a)l_1(a)}\right)^2 \tag{12}$$

*Corollary 2: $T'_{ST}$ is a negative definite function whose magnitude is constrained depending on the dimensionless normalized damping coefficient, $\mu$,*

$$\begin{array}{lcl} \mu > 0 & \Leftrightarrow & -T'_{ST}(a^*) \in (0, 1) \\ \mu = 0 & \Leftrightarrow & -T'_{ST}(a^*) = 1 \\ \mu < 0 & \Leftrightarrow & -T'_{ST}(a^*) \in (1, \infty) \end{array} \tag{13}$$

*Proposition 2: For $\mu > 0$, any fixed point, $r^*$, satisfying $\rho'(a^*) < 0$ has a real eigenvalue outside the unit circle for all $v^* > 0$, and therefore, is unstable.*

*Proof:*

Define a discriminant bound, $\overline{\Delta} := (1 - T'_{ST}(a^*))^2 + 4T'_{ST}(a)$, and a trace bound, $\overline{tr} := 1 - T'_{ST}(a^*)$. Corollary 2 implies that for $\mu > 0$, we have $\overline{tr} > 1$ and $\overline{\Delta} = (1 + T'_{ST}(a^*))^2 > 0$. Therefore, for $v^* > 0$ and $\rho'(a^*) < 0$, $tr > \overline{tr} > 1$ and $\Delta > \overline{\Delta} > 0$, hence, $\lambda_+ = 1/2(\, tr + \sqrt{\Delta}\,) > 1/2(\, \overline{tr} + \sqrt{\overline{\Delta}}\,) = 1$, which is on the real axis and outside the unit circle.

*Proposition 3: For $\mu > 0$, any fixed point, $r^*$, satisfying $\rho'(a^*) > 0$ has two complex conjugate eigenvalues inside the unit circle, when $v^* \in V_c := (\underline{v}, \overline{v})$, and two real eigenvalues inside the unit circle, when $v^* \in V_{sr} := (0, \underline{v}] \cup [\overline{v}, \overline{\overline{v}})$, and therefore, is stable for all $T_c$ values that results in $v^* \in V_s$, where*

$$V_s := (0, \overline{\overline{v}}). \tag{14}$$

*and $\underline{v}$, $\overline{v}$, and $\overline{\overline{v}}$ are defined in the proof below.*

*Proof:*

Since $\rho'(a^*) > 0$, $\Delta$ is a quadratic function of $v^*$ possessing two positive roots, $0 < \underline{v} < \overline{v}$. We partition the touchdown speed space, $\mathbb{R}^+$, into 3 cells according to the sign of $\Delta$: $V_{r1} := (0, \underline{v}] = \{v^* | 0 \le \Delta(v^*) < \overline{\Delta}\}$; $V_c := (\underline{v}, \overline{v}) = \{v^* | \Delta(v^*) < 0\}$; and $V_{r2} := (\overline{v}, \infty) = \{v^* | \Delta(v^*) \ge 0\}$.

For all $v^* \in V_{r1}$, the discriminant and trace are monotonically decreasing and bounded by $0 < 2\sqrt{-T'_{ST}(a^*)} < tr < 1 - T'_{ST}(a^*)$, $0 < \Delta \le \overline{\Delta}$. Therefore, the eigenvalues are real, and inside the unit circle.

For all $v^* \in V_c$, the discriminant is negative, $\Delta < 0$. Therefore, the eigenvalues of $J(a^*)$ are complex conjugate. Lemma 2 states that $|\lambda_\pm|^2 = -T'_{ST}(a^*)$, which is

known to be less than unity by Corollary 2 for $\mu > 0$. Therefore, both eigenvalue functions, $\lambda_{\pm}$, are complex and lie on the circle with radius $\sqrt{-T'_{ST}(a^*)}$ inside the unit circle.

For $v^* \in V_{r2}$ the eigenvalues are real, and by continuity, $\lambda_{\pm}(\overline{v}) = tr(\overline{v}) = -\sqrt{-T'_{ST}(a^*)} > -1$ Note that $tr$ is monotonically decreasing, and $\Delta$ is monotonically increasing for $v^* \in V_{r2}$. Let $\overline{\overline{v}} := \lambda_-^{-1}(-1)$. It follows that $\forall v^* > \overline{\overline{v}}$, $\lambda_-(v^*) < -1$. Hence, for $v^* \in (\overline{v}, \overline{\overline{v}})$ the eigenvalues are real and inside the unit circle.

*Theorem: In the presence of viscous friction, $\mu > 0$, the clock controlled 1-DOF hopper, Eq.(4), has a locally asymptotically stable limit cycle (hopping gait) for the mode sequence $\mathcal{FNAN}$, if there exists a valid $a^*$ such that $\rho(a^*) = 1$ and $\rho'(a^*) > 0$ (Eq.(10)), and $T_c$ is chosen so that $v^* \in V_s$ (Eq.(14)).*

*Proof:*

For a fixed $a^*$, Eq.(11) shows that $v^*$ is completely determined by choice of $T_c$. From Proposition 3, the valid fixed point, $r^* = (v^*, a^*)$, is locally asymptotically stable, if $\rho'(a^*) > 0$, and $v^* \in V_s$ when $\mu > 0$.

*Corollary 3: If there exists a valid $a^*$ such that $\rho(a^*) = 1$ and $\rho'(a^*) > 0$, and $T_c$ is chosen so that $v^* \in V_s$, then $\mathcal{FNAN}$ contains an open positively invariant attracting subset.*

## 5. CONCLUSION

We have presented a simple vertical spring-mass hopping model modulated by a biologically inspired clock-based feedforward strategy for controlling gait — in this simple setting, steady state hopping height. Our stability results take the form of effectively computable sufficient conditions imposed upon the roots of Eq.(11). As we state in Conjecture 1, it is clear from numerical study (although not yet formally demonstrated) that these sufficient conditions are always satisfied for one and only one fixed point over a significant portion of those physically meaningful parameter values consistent with lossy operating conditions. Further, we suspect that losses in the mechanical system are necessary for stability of the coupled system when the control is imposed in this feedforward manner with no sensory feedback pathway.

The longer term goal of this research would be to leverage an understanding of more elaborate (i.e., mechanically and biologically more realistic models) from relationships between the controller parameters and the system behavior exhibited by this caricature. Moreover, we are investigating "low bit rate" feedback schemes that confer stability in the absence of mechanical losses and greatly increase the domain of attraction in all circumstances. Finally, we are looking into parallel composition and synchronization [10] of CPG-based controllers to handle mechanical systems of higher degree of freedom, such as the hypothetical SLIP [18] and physically extant Rhex [3,19].

## 6. REFERENCES


[1] Matthew D. Berkemeier and Kamal V. Desai. Control of hopping height in legged robots using a neural-mechanical approach. In *International Conference on Robotics and Automation*, pages 1695–1701, Detroit, Michigan, 1999.

[2] M. Buehler, D. E. Koditschek, and P. J. Kindlmann. Planning and control of robotic juggling and catching tasks. *International Journal of Robotics Research*, 13(2):101–118, 1994.

[3] M Buehler, U. Saranli, and D. E. Koditschek. Design, modeling and preliminary control of a compliant hexapod robot. In *ICRA*, San Fransisco, CA, 2000.

[4] H. Cruse, C. Bartling, G. Cymbalyuk, J. Dean, and M. Dreifert. A modular artificial neural net for controlling a six-legged walking system. *Biological Cybernetics*, 72:421–430, 1995.

[5] Holk Cruse, Thomas Kindermann, Michael Schumm, Jeffrey Dean, and Josef Schmitz. Walknet–a biologically ispired network to control six-legged walking. *Neural Networks*, 11(Special):1435–1447, 1998.

[6] Daniel P. Ferris, Micky Louie, and Claire T. Farley. Running in the real worl: adjusting leg stiffness for different surfaces. *Proc. R. Soc. Lond. Biological Sciences*, 265(1400):941–1044, 1998.

[7] A. V. Hill. The heat of shorthening and the dynamic constants of muscle. *Proc. R. Soc. London Ser. B*, 126:195–211, 1938.

[8] Ranu Jung, Tim Kiemel, and Avis H. Cohen. Dynamic behavior of a neural network model of locomotor control in the lamprey. *Journal of Neurophysiology*, 75(3):1074–1086, 1996.

[9] Hassan K. Khalil. *Nonlinear systems*. Prentice Hall, Upper Saddle River, NJ, 2nd edition, 1996. Hassan K. Khalil. Includes bibliographical references (p. 711-724) and indexes.

[10] Eric Klavins and Daniel E. Koditschek. Toward the regulation and composition of cyclic behaviors. In *Proceedings of 4th Int. Workshop on Algorithmic Foundations of Robotics*, Dartmouth, NH, 2000. A. K. Peters. (In Press).

[11] Nancy Kopell. Oscillating networks of neurons: mathematics and function. In *The Legacy of Norbert Wiener: A Centennial Symposium*, pages 117–136, Cambridge, MA, 1997. Amer. Math. Soc,. Paper Number CMP 1 460 279.

[12] Nancy Kopell. We got rhythm: Dynamical systems of the nervous system. *Notices of the AMS*, 47(1):6–16, January 2000 2000.

[13] Thomas A. McMahon. *Muscles, reflexes, and locomotion*. Princeton University Press, Princeton, N.J., 1984. 82023156 Thomas A. McMahon. Includes index. Bibliography: p. [311]-323.

[14] Keir Pearson. The control of walking. *Scientific American*, 464:72–86, 1976.

[15] Marc H. Raibert. *Legged robots that balance*. MIT Press series in artificial intelligence. MIT Press, Cambridge, Mass., 1986. Marc H. Raibert. Includes index. Bibliography: p. [203]-227.

[16] Robert Ringrose. Self-stabilizing running. In *International Conference on Robotics and Automation*, pages 487–493, Albuquerque, New Mexico, 1997.

[17] S. Schaal and C. G. Atkeson. Open loop stable control strategies for robot juggling. *Proceedings IEEE International Conference on Robotics and Automation (Cat. No.93CH3247-4). IEEE Comput. Soc. Press, Los Alamitos, CA, USA*, 3 vol.(xviii+1051+xvi+848+xviii+1042)):913–18 vol.3, 1993.

[18] William J. Schwind and Daniel E. Koditschek. Control of forward velocity for a simplified planar hopping robot. In *International Conference on Robotics and Automation*, 1995.

[19] Gary Taubes. Better than nature made it. *Science*, 288(5463):81, April 2000.

[20] Donald M. Wilson. Insect walking. In *Ann. Rev. Entomol,*, volume 11, pages 103–122. 1966.